A&A 483, 749–758 (2008)
DOI: 10.1051/0004-6361:20078319

Astronomy & Astrophysics

An X-ray view of absorbed *INTEGRAL* AGN

A. De Rosa[1], L. Bassani[2], P. Ubertini[1], F. Panessa[1], A. Malizia[2], A. J. Dean[3], and R. Walter[4]

[1] INAF/IASF, via del Fosso del Cavaliere 100, 00133 Roma, Italy
e-mail: alessandra.derosa@iasf-roma.inaf.it
[2] INAF/IASF, via Gobetti 101, 40129 Bologna, Italy
[3] School of Physics and Astronomy, University of Southampton Highfield, Southampton, UK
[4] INTEGRAL Science Data Centre, Chemin d'Ecogia 16, 1290 Versoix, Switzerland

Received 19 July 2007 / Accepted 5 February 2008

ABSTRACT

Aims. We present a 0.2−200 keV broadband study of absorbed Active Galactic Nuclei (AGN) observed with *INTEGRAL*, *XMM-Newton*, *Chandra*, and *ASCA* to investigate the continuum shape and the absorbing/reflecting medium properties.
Methods. The sources are selected in the *INTEGRAL* AGN sample to have a 20−100 keV flux below 8×10^{-11} erg cm^{-2} s^{-1} (5 mCrab), and are characterized by a 2−10 keV flux in the range $(0.8-10)\times10^{-11}$ erg cm^{-2} s^{-1}. The high quality of data allow us a detailed study of the intrinsic and reflected continuum components. In particular, the analysis performed on the combined broadband spectra allow us to investigate the presence of Compton reflection features and high energy cutoff in these objects.
Results. The column density of the absorbing gas establishes the Compton thin nature for three sources in which a measure of the absorption was still missing. The Compton thin nature of all the sources in this small sample is also confirmed by the diagnostic ratios F_x/F [OIII]. The Compton reflection components we measure, reflection continuum and iron line, are not immediately compatible with a scenario in which the absorbing and reflecting media are one and the same, i.e. the obscuring torus. A possible solution is that the absorption is more effective than reflection, e.g. under the hypothesis that the absorbing/reflecting medium is not uniform, like a clumpy torus, or that the source is observed through a torus with a very shallow opening angle. The high energy cutoff (a lower limit in two cases) is found in all sources of our sample and the range of values is in good agreement with that found in type 1 Seyfert galaxies. At lower energies there is clear evidence of a soft component (reproduced with a thermal and/or scattering model), in six objects.

Key words. X-rays: galaxies – galaxies: Seyfert – galaxies: nuclei

1. Introduction

The broadband properties of Seyfert 2 AGN have been extensively studied in previous years, mainly using *Beppo-SAX* data (Risaliti 2002). The continuum shape in these objects can be reproduced by a steep power-law with photon index $\Gamma \sim 2$. This model matches a Comptonization scenario in which seed photons from a cold gas (the accretion disc) are up-scattered in a hot corona of relativistic electrons (Haardt & Maraschi 1991; Haardt et al. 1997). A photoelectric cutoff is present at X-ray energies and its value depends on the absorbing column density of the source. For N_H in the $10^{22}-10^{23}$ cm^{-2} range, the cutoff is below 2 keV, for N_H in the $10^{23}-10^{24}$ cm^{-2} range, the cutoff is in 3−10 keV band and for $N_H > \sigma_T^{-1} = 1.5\times10^{24}$ cm^{-2} (i.e., the Compton-thick regime with σ_T^{-1} being the inverse of the Thomson cross section), the continuum can be observed only through its reflected component above 10 keV.

The presence of a high-energy cutoff is still an open issue. Risaliti (2002) found that the high energy cutoff is present only in ∼30 per cent of a sample of 20 bright Sy 2 observed with *Beppo-SAX*. Above 10 keV the presence of a Compton reflection component has often been observed, however, its origin is still unclear as well as if the reflecting/absorbing medium are one and the same (the putative "molecular torus"). A cold iron line at 6.4 keV is often associated with this continuum Compton reflection hump.

The IBIS gamma-ray imager on board *INTEGRAL* is surveying the whole sky above 20 keV with a mCrab (∼10^{-11} erg cm^{-2} s^{-1}) sensitivity in well exposed regions. With its angular resolution of 12 arcmin and the point source location accuracy of 1−2 arcmin for moderately bright sources (Ubertini et al. 2003), *INTEGRAL* has already detected a number of AGN, a large fraction of which were previously unknown as high-energy emitters (Bird et al. 2006; Bassani et al. 2006a; Bird et al. 2007).

In this paper, we present a deep broadband spectral analysis of seven absorbed AGN detected by *INTEGRAL*. The sample is extracted from the Bassani et al. (2006a) survey, updated to include a number of optical classifications obtained afterward (see Bassani et al. 2006b). The sample includes Seyfert 2 galaxies, having a 20−100 keV flux below 5 mCrab, and X-ray data available at the time this work started. From the sample, we have excluded sources already studied by *Beppo-SAX* except for one object (ESO 103-G35), which was retained to provide a direct comparison between this work and previous studies using *Beppo-SAX* data and allowed us to make an a posteriori check of our analysis procedure, which is affected by the limitation of using nonsimultaneous X- and soft gamma-rays data. Overall, we can conclude that the sample used in this study is representative of the population of type 2 AGN detected by *INTEGRAL* above 10 keV; further broadband X/gamma-ray analysis on a complete sample of type 2 AGN selected in the 20−40 keV

band is ongoing and will be the objective of a future paper[1]. Four sources (IGR J12391-1610 = LEDA170194 hereafter, IGR J07565-4139, IGR J12026-5349, and IGR J10404-4625) have been discovered first in soft gamma-ray band and immediately after observed with *Chandra* (LEDA170194, IGR J07565-4139, and IGR J12026-5349) and *XMM-Newton* (IGR J10404-4625). Two objects (ESO 103-G35 and IC 4518A) are known AGN (although IC 4518A was never reported at X-ray energies before) and follow-up observations with *XMM-Newton* have been used in our broadband analysis. For one object, (NGC 788) archival *ASCA* data have been used in this work. Using X-ray measurements, in conjunction with *INTEGRAL* data, allow us to build a spectrum in three decades of energy, and to distinguish between the various spectral components characterizing the broadband spectra of absorbed AGN. This in turn will allow us, in particular, to study the absorption/reflection medium properties of the sample. These good quality spectra also permit a detailed investigation of the intrinsic continuum slope including the cutoff if present. The broadband coverage available is a powerful and unique tool to address all these issues, making possible a simultaneous measurement of the intrinsic continuum (both photon index and high energy cutoff) and of the reflected continuum together with the Fe line.

Note that a number of sources in the sample have data already published in the literature both in the X-ray band (Sazonov et al. 2005; Shinozaki et al. 2006) and in soft gamma-ray range (Beckmann et al. 2006; Molina et al. 2006). However, most of these works did not provide a detailed analysis of the broadband spectra of the sources in the sample nor attempt to put constraints on the high energy cutoff and reflection bump. The only exception is ESO 103-G35 analysed by our team with *Beppo-SAX* and *INTEGRAL* data; here we use a recent *XMM-Newton* observation of the source in conjunction with an updated *INTEGRAL* spectrum to have a well studied object to use as a source of reference in the sample.

In Sect. 2, we present the data of our small sample, while the models used to fit the spectra are described in Sect. 3. We present results and discussion in Sect. 4, and draw our conclusions. In the appendix, we discuss single cases in more detail.

2. Observations and data reduction

2.1. INTEGRAL data

The AGN discussed here have been observed with IBIS (Ubertini et al. 2003), the imager on board *INTEGRAL* (Winkler et al. 2003). This coded mask instrument is made by combining two detector layers: ISGRI (Lebrun et al. 2003), an upper CdTe layer sensitive in the range between 15 keV and 1 MeV, and PICsIT (Di Cocco et al. 2003), a bottom CsI layer sensitive in the range 200 keV to 8 MeV. In the present paper, we refer to data collected by the first layer only, since the sources are too weak above ∼100 keV for detection by PICsIT.

For each source, we combined *INTEGRAL* data from several pointings performed between revolution 12 and 429 to provide sufficient statistics. First we generated *ISGRI* images for each available pointing in 13 energy bands with the ISDC offline scientific analysis software OSA version 5.1. Then, we extracted count rates at each source position from individual images to provide light curves in the various energy bands sampled; since the light curves did not show any sign of variability or flaring activity, average fluxes were then extracted in each band and combined to produce the source spectrum. A detailed description of the source extraction criteria can be found in Bird et al. (2006, 2007). We have tested that this method of spectral extraction is reliable by comparing the Crab spectrum obtained in this way with the one extracted with the standard spectral analysis.

In Table 1, we report the details of the IBIS/ISGRI observations; best fit positions, exposures and count rates in the range 20−100 keV. The positional uncertainty for sources of this intensity is around ∼3 arcmin (Bird et al. 2006).

2.2. Chandra data

Chandra observed LEDA170194 on July 25, 2005, and IGR J12026-5349 and IGR J07565-4139 on June 16, 2005, with ACIS-I. Details on the observations are given in Table 1. We reduced data with CIAO v3.2, following standard procedures. It is important to note here that although Sazonov et al. (2005) used *Chandra* spectra in conjunction with *INTEGRAL* data, they did not attempt to estimate cutoff energy and reflection bump in their analysis, probably due to the limited amount of spectral information available above 10 keV (a single bin in the 17−60 keV band). All *Chandra* sources suffer from pile-up. Using WebPIMMS[2], we estimated the fraction of pile-up to be around 36 per cent for IGR J07565-4139; 30 per cent for IGR J12026-5349; and >20 per cent for LEDA170194. The effect of pileup is clearly visible through a hardening of the spectrum above 4.5−5 keV. Regarding the pile-up problem, we point out that we have used a different approach than the one adopted by Sazonov et al. (2005): these authors removed the central pixel, i.e.,excluding 80% of the instrument PSF, and consequently used data up to 5 keV. We have instead maintained the central pixel and dealt with the spectra affected by pile-up through the PILE-UP model available in XSPEC, which can correct the total spectrum for the pile-up effects, provided that this is less than 70% (Davis 2001).

2.3. XMM-Newton data

We also observed with *XMM-Newton* EPIC ESO 103-G35, IC 4518A and IGR J10404-4625. Details on the observations are given in Table 1. We reduced the data reduction with version 7.0 of the SAS software, employing the most updated calibration files available at the time of the data reduction (2006 March). We empoyed patterns 0 to 12 (4) in the extraction of the MOS (pn), scientific products. In the case of IC 4518A pn and MOS, spectra for the source were extracted from a circular region of 30 arcsec radius while background spectra were taken from source-free circular regions of 10 arcsec radius. In the case of ESO 103-G35 MOS (pn) spectra were extracted from a circular region of 35 (60) arcsec radius around the source while background spectra were taken from source-free circular regions of 10 (40) arcsec radius. Finally, in the case of IGR J10404-4625 MOS (pn) spectra were extracted from a circular region of 40 (90) arcsec radius around the source, while background spectra were extracted from source-free circular regions of 20 (40) arcsec radius. Spectra are rebinned to have at least 20 counts

[1] 6 other type 2 AGN from Bassani et al. survey are below the assumed threshold flux: 3 (IGR J12415+5750, IGR J20286+2544, and IGR J17513-2011) had no X-ray data available when this analysis started while 3 (NGC 1068, Mkn 3, and NGC 6300) had BeppoSAX observational results published. However all three are peculiar objects, the first two being Compton thick AGN, and the third one the prototype of "changing look" Seyfert 2 (i.e., a source that goes from thick to thin and vice versa).

[2] http://heasarc.gsfc.nasa.gov/Tools/w3pimms.html

Table 1. Journal of the observations.

Name	Mission	Date	Exp time (s)	RA, Dec (J2000) (h m s, °′″)	Counts (s^{-1})
LEDA170194	*Chandra*	2005/07/25	3213	12 39 06.24, –16 11 56.4	$^{\star}0.063 \pm 0.005$
LEDA170194	*INTEGRAL*	–	200 000	12 39 11.04, –16 10 55.2	$^{\circ}0.76 \pm 0.09$
IGR J07565-4139	*Chandra*	2005/06/16	3216	07 56 15.36, –41 38 09.6	$^{\star}0.215 \pm 0.008$
IGR J07565-4139	*INTEGRAL*	–	968 000	07 56 29.52, –41 38 31.2	$^{\circ}0.16 \pm 0.03$
IGR J12026-5349	*Chandra*	2005/06/16	3220	12 02 36.72, –53 49 12.0	$^{\star}0.209 \pm 0.008$
IGR J12026-5349	*INTEGRAL*	–	728 000	12 02 50.16, –53 49 12.0	$^{\circ}0.47 \pm 0.05$
NGC 788	*ASCA*	1999/01/16–18	39 160	02 01 04.30, –06 52 48.0	$^{\dagger}0.024 \pm 0.001$
NGC 788	*INTEGRAL*	–	594 000	02 01 03.36, –06 48 50.4	$^{\circ}0.85 \pm 0.07$
ESO 103-G35	*XMM-Newton*	2002/03/15	11 987	18 38 08.30, –65 24 28.8	$^{\ddagger}0.507 \pm 0.007(1.71 \pm 0.01)$
ESO 103-G35	*INTEGRAL*	–	44 000	18 38 46.80, –65 24 28.8	$^{\circ}0.84 \pm 0.13$
IC 4518A	*XMM-Newton*	2006/08/07	11 460	14 57 44.32, –43 09 33.8	$^{\ddagger}0.061 \pm 0.03(0.218 \pm 0.007)$
IC 4518A	*INTEGRAL*	–	898 000	14 57 38.40, –43 07 44.4	$^{\circ}0.293 \pm 0.03$
IGR J10404-4625	*XMM-Newton*	2006/11/29	13 530	10 40 22.32, –46 25 25.6	$^{\ddagger}\ 0434 \pm 0.003(1.40 \pm 0.01)$
IGR J10404-4625	*INTEGRAL*	–	626 000	10 40 25.68, –46 24 36.0	$^{\circ}0.283 \pm 0.04$

* In 1−7 keV. † In 2−10 keV for SIS0. ‡ In 0.5−10 keV for MOS(pn). $^{\circ}$ In 20−100 keV for IBIS/ISGRI.

in each spectral channel. Spectral fit were performed simultaneously with MOS1, MOS2 and pn in 0.5−10 keV. Cross-calibration constant pn/MOS1 and MOS2/MOS1 were left free to vary and always found in the range 0.97−1.04. *XMM-Newton* data of ESO 103-G35 have been already published in Shinozaki et al. (2006). Their analysis was restricted to 0.5−10 keV energy range and is consequently not conclusive about Compton reflection and high energy cutoff. In Appendix A we will also discuss our results about absorption in comparison with those presented in Shinozaki et al. (2006).

2.4. ASCA data

We finally analysed an archival *ASCA* spectrum of NGC 788. We downloaded the relevant spectra and associated files from the TARTARUS archive[3]. We fitted the spectra of all instruments SIS0, SIS1, GIS2, and GIS3 simultaneously in the 0.6−10 keV band. The cross-calibration constant between the different instruments were left free during the fit, and found in the range SIS1/SIS0 = $1.06^{+0.11}_{-0.11}$, GIS2/SIS0 = $0.96^{+0.10}_{-0.09}$, GIS3/SIS0 = $1.09^{+0.10}_{-0.09}$.

3. Spectral fitting

We performed spectral analysis with XSPEC v11.3. Errors correspond to the 90 percent confidence level for one interesting parameter ($\Delta\chi^2 = 2.7$). We fitted simultaneously the soft and hard X-ray spectra available with *INTEGRAL* and either *Chandra*, or *XMM-Newton* or *ASCA*. We fixed the cross-calibration constant between *INTEGRAL* and the low energies instruments ($C_{INTEGRAL}$) to 1. Possible miscalibration between *INTEGRAL* and *XMM-Newton*, *Chandra* or *ASCA* (i.e. $C_{INTEGRAL} \neq 1$) can mimic or hide the presence of a Compton reflection component above 10 keV. We choose to put this constant equal to one for all spectra because we found a good fit with this value (all reduced χ^2 around 1). However, in Sect. 4 we discuss the implications on our fit if $C_{INTEGRAL}$ is left free to vary.

To reproduce the broadband spectra of our sample, we employed three different models. The first one (Model A) consists of an intrinsic absorbed power-law, a thermal soft X-ray component and a Gaussian emission (Fe) line. The data and data/model A ratio for all source is shown in Fig. 1. In the second model (Model B), we added to the primary emission a high energy cutoff; in this case we modelled the primary emission with an e-folded power-law (CUTOFFPL model in XSPEC). In the third model (Model C), we added to the previous continuum a Compton reflection component; in this model the primary emission is modelled with an e-folded power-law plus reflection from an infinite cold slab. In the Compton reflection component (PEXRAV model in XSPEC, Magdziarz & Zdziarski 1995), the cosine of the inclination angle of the reflector was fixed to 0.95. We assume elemental abundances from Anders & Grevesse (1989). In the case of LEDA170194, IGR J07565-4139, and IGR J12026-5349 we choose to fix in all models the photon index $\Gamma = 1.7$, i. e., the average value observed in AGN, the energy of the Fe line $E_{\rm Fe} = 6.4$ keV and the intrinsic width of the line $\sigma_{\rm Fe} = 10$ eV. These assumptions are needed because the low statistics of *Chandra* data did not allow us to constrain simultaneously all the parameters of the models, Γ, $E_{\rm cut}$, and reflection.

The results of the fitting procedure with model A, B, and C are presented in Tables 2−4 respectively.

4. Results and discussion

All our models provide a good fit to all spectra, with χ^2/d.o.f. around 1. Model A, B, and C have, in fact, an average reduced χ^2 value of 0.97, 0.92, and 0.90 respectively. Here we present the main results of our analysis.

4.1. The soft X-ray spectra

All sources with the exception of IGR J07565-4139 show evidence of an unabsorbed component at energies less than 2 keV. Recent high-resolution spectroscopic data available with *XMM-Newton* on bright absorbed AGN (Massaro et al. 2006; Guainazzi & Bianchi 2007) show evidence that the soft excess component is dominated by emission lines and originates in a gas photoionized by the primary continuum in which the density is decreasing with radius like r^{-2}, as observed in the Narrow Line Region (NLR). In addition, high resolution images available with *Chandra*, show that in some cases (e.g., NGC 4549

[3] http://tartarus.gsfc.nasa.gov

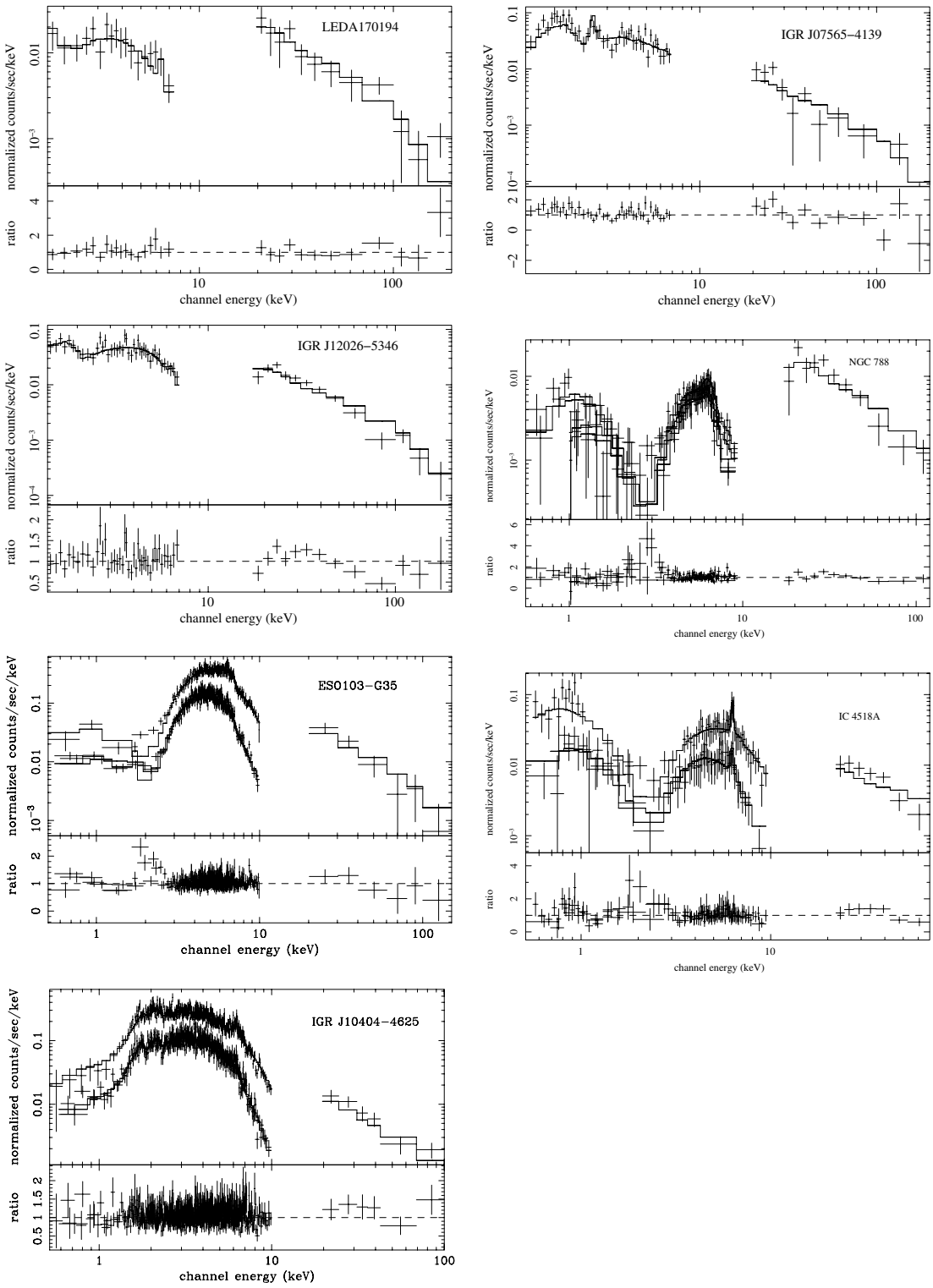

Fig. 1. Spectra and data/model ratio for all sources of our sample. The ratios are plotted using our model A: absorbed power-law+thermal emission+iron line.

Schurch et al. 2002) the soft X-ray emission has a thermal origin and is dominated by a starburst component. We have therefore taken two approaches, in the first we modelled the soft excess with a thermal component, i.e. a black-body model. With only one exception, the temperatures we found are in the range 0.2−0.9 keV (see Table 2); in the case of IGR J12026-5349 the value of $kT = 1.7^{+0.1}_{-0.2}$ keV is much higher than typically observed in type 2 AGN. In the second, we investigated the alternative scenario in which the soft X-ray excess is reproduced by a scattered component, i.e., a power-law having the same photon index of the nuclear continuum but a different normalization. In this case, we still obtain a good fit in the case of LEDA170194, NGC 788, ESO 103-G35, IC 4518A, and IGR J10404-4625 (χ^2/d.o.f. are 25/25, 291/298, 1081/1102, 102/126, and 1136/1071, respectively to be compared with those in Table 2). The only exception is again IGR J12026-5349. The

Table 2. Model A composed by an absorbed power-law component, a thermal soft emission and a Gaussian iron line.

	$^1N_{\rm H}^{\rm gal}$	$^1N_{\rm H}$	Γ	$A_{\rm soft}/A_{\rm IC}$	$^2KT_{\rm soft}$	$^2E_{\rm line}$	$^2\sigma_{\rm line}$	$^3EW_{\rm line}$	$^4F^{\rm unabs}_{2-10\ \rm keV}$	$^4F_{20-100\ \rm keV}$	χ^2/d.o.f.
LEDA170194	0.0369	$4.4^{+1.2}_{-1.5}$	1.7⋆	0.01	$0.9^{+0.1}_{-0.1}$	6.4⋆	0.01⋆	<1000	2.7	4.9	16/24
IGR J07565-4139	0.458	$0.4^{+0.2}_{-0.2}$	1.7⋆	–	–	6.4⋆	0.01⋆	<548	0.8	1.5	68/51
						2.4 ± 0.5	<0.2	109^{+88}_{-78}			
IGR J12026-5349	0.164	31^{+120}_{-27}	1.7⋆	0.12	$1.7^{+0.1}_{-0.2}$	6.4⋆	0.01⋆	<3000	10	3.9	57/50
NGC 788	0.0217	40^{+6}_{-2}	$1.6^{+0.1}_{-0.1}$	0.01	$0.30^{+0.10}_{-0.07}$	$6.3^{+0.1}_{-0.1}$	$0.27^{+0.23}_{-0.15}$	243^{+177}_{-80}	1.7	3.8	304/297
ESO 103-G35	0.0764	$18.8^{+0.7}_{-0.7}$	$1.88^{+0.06}_{-0.07}$	0.002	$0.28^{+0.05}_{-0.04}$	$6.3^{+0.1}_{-0.1}$	$0.47^{+0.11}_{-0.11}$	197^{+33}_{-33}	6.1	7.9	1078/1101
IC 4518A	0.09	$15.0^{+1.7}_{-2.7}$	$1.3^{+0.1}_{-0.1}$	0.03	$0.22^{+0.03}_{-0.03}$	$6.26^{+0.07}_{-0.14}$	<0.3	335^{+197}_{-166}	0.58	2.9	76/125
IGR J10404-4625	0.137	$4.1^{+0.3}_{-0.1}$	$1.83^{+0.06}_{-0.05}$	0.009	$0.39^{+0.08}_{-0.08}$	$6.21^{+0.05}_{-0.07}$	$0.19^{+0.11}_{-0.06}$	209^{+67}_{-50}	1.7	2.5	1132/1070

[1] In 10^{22} cm^{-2}. [2] In keV. [3] In eV. [4] In 10^{-11} erg cm^{-2} s^{-1}. ⋆ Frozen during the fit.

Table 3. Model B composed by an absorbed power-law component with high energy exponential cutoff, a thermal soft emission and a Gaussian iron line.

	$^1N_{\rm H}$	Γ	$^2E_{\rm c}$	$^2KT_{\rm soft}$	$^2E_{\rm line}$	$^3EW_{\rm line}$	$^2\sigma_{\rm line}$	χ^2/d.o.f.
LEDA170194	$4.2^{+1.5}_{-1.5}$	1.7⋆	>160	$1.1^{+2.9}_{-0.3}$	6.4⋆	<1600	0.01⋆	18/23
IGR J07565-4139	$0.5^{+0.2}_{-0.3}$	1.7⋆	>80	–	6.4⋆	<540	0.01⋆	58/50
					$2.4^{+0.2}_{-0.1}$	108^{+92}_{-71}	<0.2	
IGR J12026-5349	15^{+39}_{-13}	1.7⋆	83^{+167}_{-13}	$1.6^{+0.3}_{-0.1}$	6.4⋆	<2000	0.01⋆	43/49
NGC 788	$33.8^{+2.8}_{-3.6}$	$1.3^{+0.3}_{-0.1}$	60^{+50}_{-20}	$0.29^{+0.10}_{-0.08}$	$6.3^{+0.1}_{-0.1}$	334^{+84}_{-103}	$0.4^{+0.2}_{-0.1}$	297/296
ESO 103-G35	$18.6^{+0.8}_{-0.8}$	$1.82^{+0.09}_{-0.15}$	>70	$0.28^{+0.04}_{-0.04}$	$6.28^{+0.11}_{-0.10}$	189^{+63}_{-50}	$0.47^{+0.13}_{-0.11}$	1076/1100
IC 4518A	15^{+3}_{-2}	$1.2^{+0.1}_{-0.2}$	133^{+280}_{-75}	$0.22^{+0.03}_{-0.03}$	$6.27^{+0.07}_{-0.13}$	297^{+184}_{-141}	<1.0	74/124
IGR J10404-4625	$4.10^{+0.03}_{-0.07}$	$1.82^{+0.04}_{-0.06}$	>170	$0.39^{+0.10}_{-0.07}$	$6.21^{+0.05}_{-0.07}$	210^{+65}_{-48}	$0.19^{+0.11}_{-0.04}$	1132/1069

[1] In 10^{22} cm^{-2}. [2] In keV. [3] In eV. [4] In 10^{-11} erg cm^{-2} s^{-1}. ⋆ Frozen during the fit.

Table 4. Model C composed by an absorbed e-folded power-law component, a reflection from a cold slab, a thermal soft emission and a Gaussian iron line.

	$^1N_{\rm H}$	Γ	$^2E_{\rm C}$	$^\dagger R$	$^2KT_{\rm soft}$	$^2E_{\rm Line}$	$^3EW_{\rm line}$	$^2\sigma_{\rm line}$	χ^2/d.o.f.
LEDA170194	$2.9^{+1.3}_{-0.3}$	1.7⋆	>210	<2.4(<2.4)	$1.3^{+1.7}_{-0.3}$	6.4⋆	<1800	0.01⋆	18/22
IGR J07565-4139	$0.4^{+0.2}_{-0.3}$	1.7⋆	40^{+160}_{-10}	<7 (<7)	–	6.4⋆	<621	0.01⋆	55/49
						$2.46^{+0.08}_{-0.05}$	184^{+87}_{-76}	<0.2	
IGR J12026-5349	$3.3^{+41}_{-2.7}$	1.7⋆	170^{+130}_{-50}	$1.3^{+5.7}_{-0.4}$ ($1.3^{+6.7}_{-1.2}$)	$1.8^{+0.3}_{-0.3}$	6.4⋆	<3000	0.01⋆	40/48
NGC 788	30^{+6}_{-3}	$1.25^{+0.05}_{-0.17}$	62^{+38}_{-24}	$0.9^{+1.3}_{-0.7}$ (<2.5)	$0.29^{+0.11}_{-0.06}$	$6.31^{+0.11}_{-0.13}$	539^{+231}_{-109}	$0.44^{+0.28}_{-0.29}$	296/295
ESO 103-G35	$18.9^{+0.6}_{-1.1}$	$1.9^{+0.2}_{-0.2}$	50^{+250}_{-25}	$1.7^{+0.6}_{-0.5}$ ($2.1^{+1.5}_{-1.1}$)	$0.28^{+0.04}_{-0.03}$	$6.27^{+0.11}_{-0.12}$	325^{+100}_{-100}	<0.06	1062/1099
IC 4518A	14^{+3}_{-1}	$1.5^{+0.2}_{-0.3}$	70^{+60}_{-30}	$2.6^{+3.5}_{-1.5}$ ($1.9^{+1.3}_{-1.3}$)	$0.23^{+0.03}_{-0.02}$	$6.28^{+0.05}_{-0.05}$	360^{+106}_{-190}	< 0.35	67/123
IGR J10404-4625	$4.6^{+0.3}_{-0.4}$	$1.95^{+0.28}_{-0.07}$	>120	$1.1^{+2.4}_{-0.7}$ ($2.2^{+3.2}_{-1.5}$)	$0.39^{+0.20}_{-0.05}$	$6.22^{+0.03}_{-0.06}$	215^{+70}_{-80}	$0.13^{+0.12}_{-0.06}$	1120/1068

[1] In 10^{22} cm^{-2}. [2] In keV. [3] In eV. [4] In 10^{-11} erg cm^{-2} s^{-1}. ⋆ Frozen during the fit. † Reflection fraction obtained with $C_{INTEGRAL} = 1$ and $C_{INTEGRAL}$ free to vary (in the parentheses).

value of the ratio $A_{\rm IC}/A_{\rm soft}$ (relative to the case where the soft and hard photon indices are frozen to the same value) for all sources is listed in Table 2. This value provides an estimate of the relative strength of the soft excess with respect to the primary emission. The ratios in Table 2 are of the order of a few percent for those sources that are well reproduced by a soft power-law component; this value is also in good agreement with the value measured in a sample of absorbed AGN observed with *XMM-Newton* and *Chandra* (Bianchi et al. 2006). This soft component is likely produced by electron scattering of the intrinsic continuum and is observed in most Seyfert 2 galaxies (Antonucci 1993; Matt et al. 1997). The evidence that the $\Gamma_{\rm soft}$ and $\Gamma_{\rm hard}$ are consistent with each other and that $A_{\rm IC}/A_{\rm soft}$ is in the expected range of values, strongly support this scenario.

In the case of IGR J12026-5349, a scattered component is not able to reproduce the soft X-ray excess (χ^2/d.o.f. = 119/51 when we substitute the thermal component with a power-law). Fitting with the scattered model *Chandra* data only, we get a good fit, however the ratio between the normalisation of the two power-laws is ∼0.12, making this scenario unlikely. The high value of kT and $A_{\rm IC}/A_{\rm soft}$ in IGR J12026-5349 give indication that the contribution of the soft excess component to the emission is higher than in the other sources. This could be due to a

starburst contribution. We will come back to this source in the appendix.

If left free to vary, the photon index of the soft component remains consistent with that of the primary emission in the case of LEDA170194, ESO 103-G35, and NGC 788 ($\Gamma_{soft} = 1.0^{+0.9}_{-0.7}$, $\Gamma_{soft} = 1.8^{+0.4}_{-0.2}$, and $\Gamma_{soft} = 2.1^{+0.5}_{-0.5}$ respectively to be compared with the values in Table 2). This supports the "scattered" scenario for these three sources. On the contrary, for IC 4518A, if left free to vary, the photon index of the soft unabsorbed component is steeper with respect to that of the absorbed one ($\Gamma_{soft} = 2.7^{+0.4}_{-0.4}$), suggesting that in this case the soft X-ray component could be of thermal origin. In the case of IGR J10404-4625 the soft photon index instead gets harder than that of the nuclear component ($\Gamma_{soft} = 0.9^{+0.2}_{-0.1}$); such a hard value is probably related to the presence of the Compton hump above 10 keV. This clearly shows the importance of fitting simultaneously the data from 0.5 to 200 keV.

IGR J07565-4139 is a peculiar case, as in this source we do not find evidence for "continuum" soft X-ray emission. A narrow emission line at $2.46^{+0.08}_{-0.05}$ keV is required in the model for this source; the line has an equivalent width of 184^{+87}_{-76} eV with respect to the unabsorbed continuum (see Table 4; model C represents the best fit in the case of IGR J07565-4139). The energy of the line suggests that it could be due to K_α fluorescence of highly ionized elements like S or Si (SXV, with the theoretical value of energy of 2.430 keV, and SiXIV, with the theoretical value of energy of 2.461 keV), and could be produced in a scattering warm gas photoionized by the primary emission, as already observed in other obscured AGN such as NGC 1068 and the Circinus galaxy (Guainazzi et al. 1999; Massaro et al. 2006). The lack of any other emission feature due to high ionized elements prevents the creation of a ionization structure for this gas. If we assume that the warm medium has $N_H \sim 10^{22}$ cm^{-2} and ionization parameter U_X (defined as the ratio between the density of ionizing photons and the gas density) in the range in 0.1−5, we can produce the observed line. This gas could be associated with the NLR and/or the [OIII] ionization cones as demonstrated to be the case for other obscured AGN (Bianchi et al. 2006).

4.2. Absorption

We measured column density in excess the Galactic value was measured in all sources, as expected in type 2 Seyfert galaxies. The minimum and maximum values of N_H in our sample are 0.1 and 40×10^{22} cm^{-2}, respectively, with an average value $\bar{N}_H = (10.6^{+0.2}_{-0.2}) \times 10^{22}$ cm^{-2} (see Table 4). For all our sources, we have also estimated the F_X/F[OIII]λ5007 ratios (see Table 5). The flux of [OIII]λ5007 has been corrected for intrinsic galactic reddening following the prescription of Bassani et al. (1999) and is used here as an isotropic indicator of the intrinsic brightness of each source. We find that all F_X/[OIII] ratios are indeed well above those measured in Compton thick sources and comparable with those observed in type 1 AGN (Bassani et al. 1999). The column densities measured, as well as the F_X/F[OIII]λ5007 ratios shown in Table 5 allow us to confirm the already established Compton thin nature in the case of LEDA170194, IGR J07565-4139, IGR J12026-5349, and ESO 103-G35, and to establish that also NGC 788, IC 4518A, and IGR J10404-4625 are Compton thin AGN.

Malizia et al. (2007) recently analysed a sample of AGN observed with *INTEGRAL* and *Swift*/BAT providing a diagnostic tool (*Flux* (2−10 keV)/F(20−100 keV) softness ratio) to isolate peculiar objects and to investigate their Compton thin/thick nature. With this new tool, they were able to reconfirm the Compton thin nature of all our sources, but identified IGR J07565-4139 as a peculiar object as its location in this new diagnostic plot was outside the expected trend.

Table 5. Fux of [OIII] λ5007 corrected for absorption and its ratio with the unabsorbed flux in 2−10 keV.

Source	$^\star F$([OIII])	F_X/F[OIII]	Ref.
LEDA170194	0.55	4.9	(1)
IGR J07565-4139	<0.02	>40	(2)
IGR J12026-5349	0.2454	40.7	(2)
NGC 788	0.027	62.9	(3)
ESO 103-G35	0.112	54.5	(4)
IC 4518A	–	–	–
IGR J10404-4625	0.004	425	(5)

* In 10^{-11} erg cm^{-2} s^{-1}. (1) Masetti et al. (2006a). (2) Masetti et al. (2006c). (3) Vaceli et al. (1997). (4) Bassani et al. (1999). (5) Masetti et al. (2006b).

4.3. The reflecting medium, the origin of the Compton bump and of the iron line

We measure the reflection fraction through the parameter R that represents the ratio between the reflected and primary components. The model (PEXRAV, Magdziarz & Zdziarski 1995) assumes a perfect reflection from an infinite slab covering 2π angle. This means that in the case of a face-on line of sight, R has to be in the range 0−2. The importance of the reflection component is shown in a comparison between Tables 3 and 4. The addition of one interesting parameter, R in model C, with respect to model B is statistically required in the case of ESO 103-G35, IC 4518A, and IGR J10404-4625, with a significance of 99.98, 99.95, and 99.93 percent respectively, according to the standard F-test. In the case of IGR J12026-5349 and NGC 788, R is constrained but with a F-test probability of only 93.6 and 99.1 per cent respectively. In the case of LEDA170194 and IGR J07565-4139, we are only able to find an upper limit to R even if with an unphysical value greater than 2. We will return to this point later. In Fig. 2, we plot the reflection fraction R versus the photon index Γ. The values of R we obtain are in good agreement with those found in the *Beppo-SAX* sample of type 2 AGN (Risaliti 2002); *Beppo-SAX* average values are also shown in Fig. 2. IC 4518A and NGC 788 show evidence of a flatter photon index than the other sources, an effect that will be discussed in Sect. 4.4 and Appendix A. No evidence for the correlation claimed by Zdziarski et al. (1999) between R and Γ is found (correlation coefficient $r = 0.0582$, suggesting no real evidences against the null hypothesis). It is important to stress here that the value of the Compton reflection fraction R is strongly dependent on the value of the cross-calibration constant $C_{INTEGRAL}$ between the soft gamma (*INTEGRAL*) and X-ray data (*Chandra*, *XMM-Newton*, and *ASCA*), which we assumed to be equal to one in all spectra. It is important to note that Kirsch and collaborators (2005) analysed the Crab spectrum observed with different instruments, and they concluded that at 20 keV the cross-calibration *XMM-Newton*/*INTEGRAL* *Chandra*/*INTEGRAL* and *ASCA*/*INTEGRAL* was close to 1 (within a few percent). This strengthens the assumption we made on $C_{INTEGRAL}$. However we also checked our assumption a posteriori. In the case of *XMM-Newton* data, if left free to vary in the model C, the cross-calibration constant MOS1/ISGRI ranges between 0.5 and 2. In

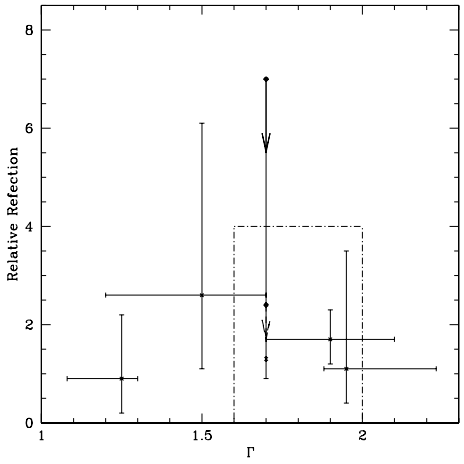

Fig. 2. Reflection fraction versus photon index in our sample. Dot-dash box shows the average values found in the *Beppo-SAX* sample of type 2 AGN (Risaliti 2002).

the case of *ASCA* data of NGC 788, $C_{INTEGRAL}$ is $0.8^{+0.6}_{-0.6}$. In the case of *Chandra* data, $C_{INTEGRAL}$ was much less constrained with respect to *XMM-Newton* and *ASCA*, mainly because of the larger gap between IBIS and ACIS (7−20 keV). In fact for *Chandra* data, if left free to vary in model C, the cross-calibration constant is found in the range 0.5−4; however, the photon index, fixed to 1.7 in the fit, still allow us to measure the reflection fraction R in IGR J12026-5349, while only upper limits are found in LEDA170194 and IGR J07565-4139. In Table 4 we report the values of R we obtain by leaving $C_{INTEGRAL}$ free to vary. It is evident that, even if the values of R are less constrained, we are able to measure the Compton Reflection in four objects, and their best fit values are not very different from those obtained with $C_{INTEGRAL} = 1$. We stress also that the errors associated to R are higher than those of Γ or kT and this is due to the degeneracy between the different spectral parameters, in particular between Γ, E_c and R. If we keep fixed Γ and/or E_c, the values of R are much more constrained with respect to those reported in Table 4 and Fig. 2.

The simplest scenario to explain the presence of the Compton hump above 10 keV in type 2 AGN, is one in which the reflecting and absorbing medium are the same, probably the putative molecular torus. Within this scenario, the question to address is if the reflection fraction we find is consistent with the absorbing column densities we measured. For $N_H = 10^{23}-10^{24}-10^{25}$ cm^{-2}, the contribution of the torus to the 30 keV flux is 8, 29, and 55 percent respectively (Ghisellini et al. 1994). This means that the value of R measured in our sources is too high to be associated only with the absorbing gas of the torus (see Table 4). A possible solution to this problem is that the absorber is not homogeneous and that a Compton thick medium covers a large fraction of the solid angle, but not the line of sight as proposed by Risaliti (2002). This absorber can be identified with the clumpy torus recently proposed to explain infrared observations of AGN and their classification in the unification theory scenario (Elitzur & Shlosman 2006).

In the case of NGC 788, ESO 103-G35, IC 4518A, and IGR J10404-4625, it has been possible to measure the Kα iron line. For the threee *Chandra* sources, LEDA170194, IGR J07565-4139, and IGR J12026-5349, we have frozen the energy of the (narrow) line $E_{Fe} = 6.4$ keV, and we were able to find only upper limits on the equivalent width. For this reason we present our conclusions about Fe line on the basis of the results we found in the other four sources. The profiles of the line when the continuum is fitted with model C, are shown in Fig. 3. The energy of the line for all the objects is consistent with neutral or little ionized iron. The line is narrow in all objects as shown by the contour plot of σ vs. Energy (see Fig. 4) obtained fitting data with Model A. In the case of ESO 103-G35, the contours plot are only marginally consistent with a narrow line profile ($\sigma = 0.47^{+0.11}_{-0.11}$ keV with Model A, see Table 2). However, when the continuum is well reproduced with Model C, in which all the spectral components are modelled, we find an upper limit to the intrinsic width of the line ($\sigma < 0.06$ keV, see Table 4 and Fig. 3) consistent with a narrow profile, as already observed by *Beppo-SAX* (Akylas et al. 2001). This underlines the importance of a good modelling of the continuum to investigate the line properties.

In Fig. 5, we plot the equivalent width versus the column density for the four sources where the Fe line has been measured. If the Fe line is produced far away from the central source, a higher value of the column density will absorb a higher fraction of the continuum at the energy of the line, but will not absorb the line photons; the total effect will be a larger value of the equivalent width. The errors on *EW* are too large to draw a solid conclusion about a possible correlation, however fitting the *EW* data shown in Fig. 5 with a constant K we found a value $K = 285 \pm 57$ eV, with χ^2/d.o.f. = 1.2. The same fit in the region below 3×10^{23} cm^{-2} gives $K = 268 \pm 60$ eV, with χ^2/d.o.f. = 1 (this best fit constant it plotted in Fig. 5 with a dashed line). The only data point with $N_H > 3 \times 10^{23}$ cm^{-2} is that of NGC 788, which has a N_H significantly higher than the other three sources. Even if we do not have enough statistics to draw any firm conclusions, we stress that the trend we find confirms the results of Risaliti (2002) on a sample of Seyfert 2 observed by *Beppo-SAX*. *Beppo-SAX* N_H average values below and above 3×10^{23} cm^{-2} are also plotted in Fig. 5. This behaviour represents strong evidence that the line has to be produced (at least in part) far away from the accretion disc, being absorbed in a different way than the continuum. The evidence of a narrow profile (see Fig. 4) strongly supports this scenario, and confirms that the best candidate for the line production site is the absorbing gas, probably a non homogeneous obscuring torus.

The question is now if the absorbing gas alone, the torus, is able to produce the observed iron lines. The value of N_H in the four sources where we measure the iron line is in the range $(4.2-36)\times10^{22}$ cm^{-2} with an average value $(16.9^{+0.2}_{-0.2})\times10^{22}$ cm^{-2} (see Table 4). A torus with column densities in this range could produce a fluorescence iron line with an average equivalent width in the range 10−200 eV and with an average value of ∼100 eV (Ghisellini et al. 1994). These values are well below those we measure suggesting that the line has to be produced, at least partly, in a gas that is different from the absorbing one. Another possibility is, again, a non homogeneous absorber not covering the line of sight uniformly. The upper limits of the equivalent width we found in the three *Chandra* spectra also support this conclusion.

The measured values of the reflection components in our sample (both iron line equivalent width and reflection continuum) suggest that the absorption is more effective than the reflection, e.g., making the hypothesis that the absorbing/reflecting medium is not uniform, likely a clumpy torus (Elitzur & Shlosman 2006). Another scenario could be that the source is observed throughout a torus with a very shallow angle. In this case the flux directly seen by the observer is due to the inverse Compton interaction of the hot plasma electrons off the seeds photons. This high energy radiation exiting the system with a

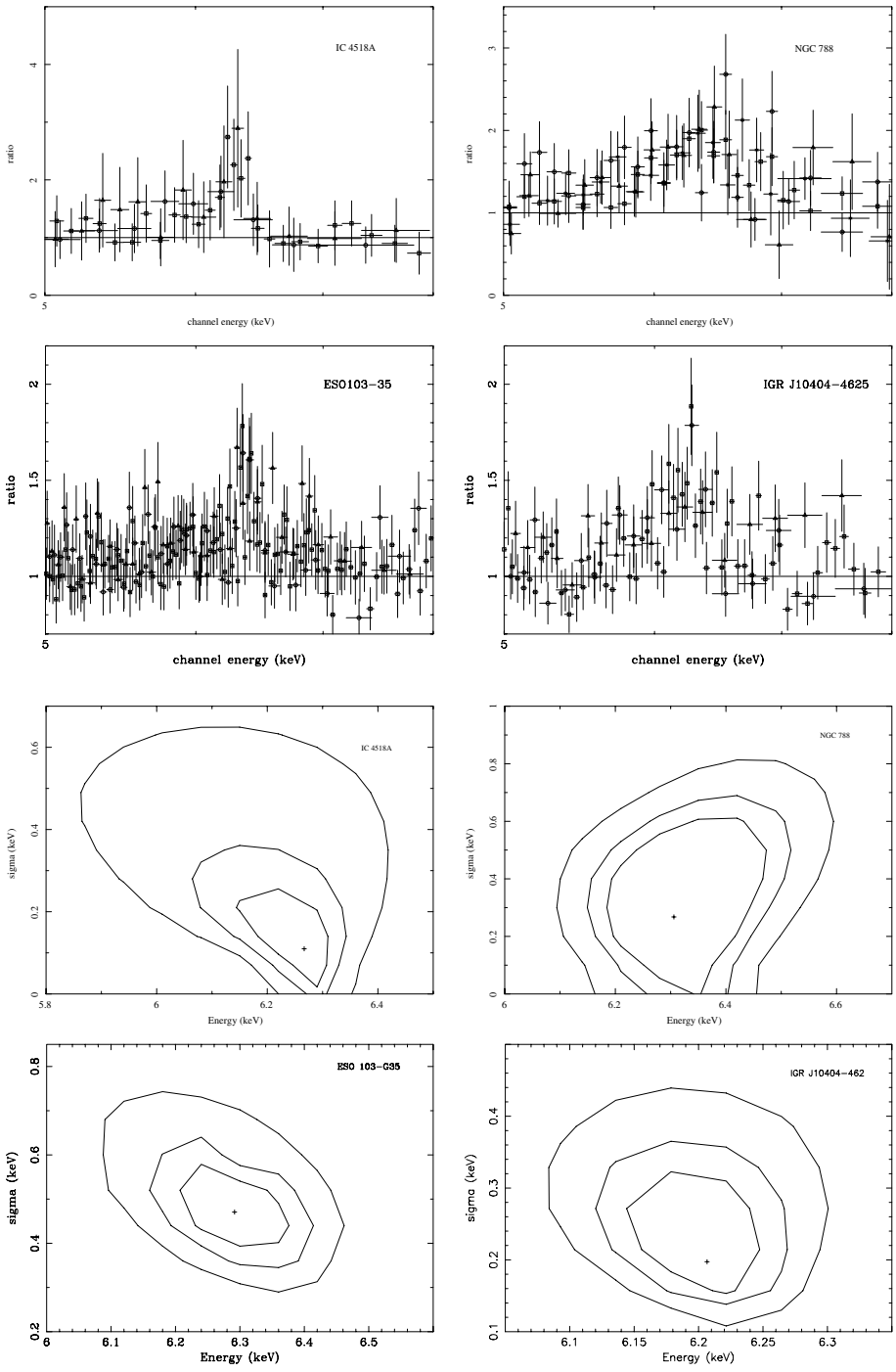

Fig. 3. The iron line profile when the continuum is reproduced with model C. For NGC 788 stars, triangles, circles and squares represents SIS0, SIS1, GIS2, and GIS3 respectively For IC 4518A, ESO 103-G35, and IGR J10404-4625 triangles, circles, and squares represent MOS1, MOS2, and pn data respectively.

Fig. 4. Contour plots 99, 90, 68 percent of the intrinsic width σ vs. Energy for the iron lines.

smaller angle with respect to the torus plan will interact with a sort of "grazing incidence" with the upper border of the torus and will see a very high column density (almost infinite). Conversely, the Compton scattered/reflected photons escaping in the direction of the line of sight, will have a Compton cone with a moderate optical path in our line of sight. This does not apply to the lower energies, which are fully absorbed anyway.

4.4. The intrinsic continuum and the high energy cutoff

We measure the high energy cutoff in five out of seven sources in the sample (see Table 4), and we find a lower limit to E_c in the case of LEDA170194 and IGR J10404-4625. All these values (either measured or lower limits) are within the range found in other Seyfert galaxies (Perola et al. 2000).

The phenomenological model we employ to fit the intrinsic continuum (i.e., power-law with a high energy cutoff), well describes a two-phase model involving a hot corona emitting medium-hard X-rays by Comptonization and a cold, optically thick layer (the disk) that provides the soft photons for the Comptonization (Haardt & Maraschi 1991; Haardt et al. 1997). In Fig. 6, we plot the high energy cutoff vs. the photon index. It is important to note that the value of E_c to be considered are those listed in Table 4 because above 10 keV the presence of Compton reflection can modify the continuum slope and, in turn, the value of the high energy cutoff (we stressed in the previous sections that there is a strong degeneracy between the reflection

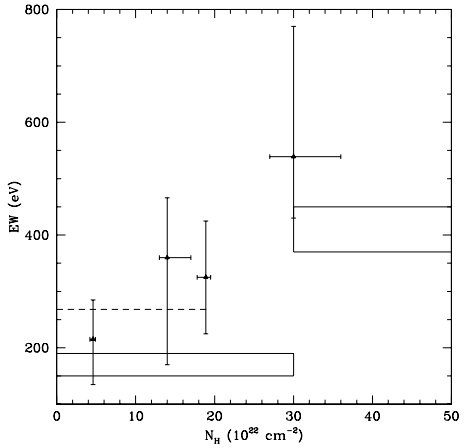

Fig. 5. Absorbing column density versus Fe equivalent width. The dotted line represent the best fit constant in the region $N_{\rm H} < 3 \times 10^{23}$ cm^{-2}. The box regions represent the average values of $N_{\rm H}$ (1σ errors) found in the *Beppo-SAX* sample of type 2 AGN (Risaliti 2002).

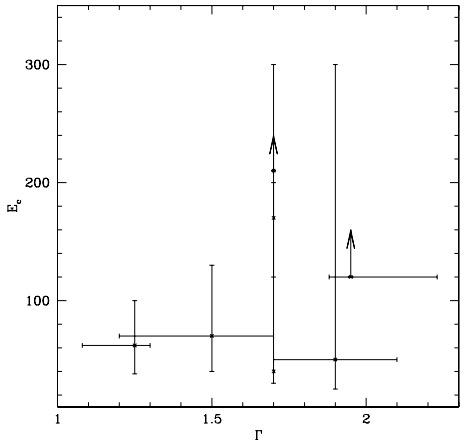

Fig. 6. High energy cutoff in keV versus photon index.

fraction R and $E_{\rm c}$). Figure 6 shows that all the values we constrain are below 300 keV, strongly suggesting the presence of a high energy cutoff in the spectra of Seyfert 2 galaxies.

In NGC 788 and IC 4518A, we find the photon index value is lower with respect to the average observed in Seyfert galaxies. The flat photon index could be either due to a bad modelling of the primary continuum, which will be discussed for the two sources in Appendix A, or it could be real, as expected in the X-ray background synthesis model (Gilli et al. 2007). To confirm the latter hypothesis we would need a larger sample.

5. Conclusions

We have presented spectral broadband analysis of a small sample of seven absorbed Seyfert 2 selected at $E > 10$ keV by *INTEGRAL*/IBIS. The combined 0.2−200 keV spectra allowed us to perform a detailed study of the emission/absorption properties and to test possible correlations between different parameters (e.g., R vs. Γ or $E_{\rm c}$ vs. Γ); in particular, for the first time in these sources, we have measured the reflection components (both Compton bump and iron line) and high energy cutoff. An a posteriori check of our analysis procedure, which is affected by the limitation of using nonsimultaneous X-ray soft gamma-ray data, is performed providing for one well known source, ESO 103-G35, which offers a direct comparison between our study and previous ones with *Beppo-SAX* data. The values of Γ, R, and $N_{\rm H}$ we found for this source are completely consistent with those obtained by Akylas et al. (2001) analysing simultaneous broadband *Beppo-SAX* observations. This evidence strengthens the validity of our fitting procedure and makes our results reliable. The main conclusions of our analysis are the followings:

- The average value of the absorbing column density is $\bar{N}_{\rm H} = (10.6^{+0.2}_{-0.2}) \times 10^{22}$ cm^{-2}, and the range observed suggests a Compton thin nature for all objects in the sample, that is a new result in the case of NGC 788, IC 4518A, and IGR J10404-4625. This evidence is also confirmed by the ratio $F_{\rm x}/F$ [OIII] λ5007.
- The continuum was reproduced with an e-folded power-law having a photon index in the range 1.3−1.9 and a high energy cutoffs well below 300 keV; this finding suggests that a cutoff is a common factor in Seyfert 2 galaxies with values in good agreement with those found in type 1 AGN.
- We measure the Compton reflection component in five sources (IGR J12026-5349, NGC 788, ESO 103-G35, IC 4518A and IGR J10404-4625) and found an upper limit in two others (LEDA170194 and IGR J07565-4139). No evidence for a correlation between R and Γ is found. We also observed the iron line (in the case of *Chandra* spectra we found upper limits only on the equivalent width). Both reflection components are not immediately consistent with production in the cold absorbing gas identified in the molecular torus. Both the reflection fraction R and the equivalent width of the line are too high to be produced in the gas with the observed column density. A possible solution is that the absorption is more effective than the reflection, e.g., making the hypothesis that the absorbing/reflecting medium is not uniform, like a clumpy torus, or that the source is observed through a torus with a very shallow opening angle.
- A soft excess component emerging below 2−3 keV is found in all sources with the only exception of IGR J07565-4139. This component is well reproduced by a thermal black body model having temperature in the range 0.2−0.9 keV, as typically observed in Sy 1. Alternatively, a power-law with photon index equal to that of the illuminating continuum is also able to reproduce this excess is some cases; the ratio of soft versus primary continuum is of the order of a few percent, as typically observed in Sy 2. A different case is that of IGR J12026-5349 which has, in the thermal model, a temperature $kT = 1.7^{+0.1}_{-0.2}$ keV and, in the scattered scenario, $A_{\rm IC}/A_{\rm soft} = 0.12$; both values are higher than observed in the other sources and, typically, in Seyfert. This strongly suggests that the source is characterized by a larger soft excess (possibly due to a starburst contribution) that is not present in the other sources.
- IGR J07565-4139 is the only source in the sample that does not show any evidence for continuum excess at low energies. A narrow emission line around 2.5 keV is instead found in the *Chandra* data.

Acknowledgements. We acknowledge the Italian Space Agency financial and programmatic support via contracts I/R/046/04 and I/023/05/0. We thank the referee for constructive suggestions.

Appendix A: Analysis of single sources

We describe the details of the analysis of each individual source; we also compare our results to previously published measurements.

LEDA170194 The fraction of pile-up estimated with PIMMs was around >20 per cent. This absorption column density we found with our broadband analysis is in good agreement with the result presented in Sazonov et al. (2005). In this source the presence of a high energy cutoff and a reflection component is not required (see Tables 2–4). We found a lower limit to E_c of ∼210 keV and an upper limit to R of ∼2.

IGR J07565-4139 The fraction of pile-up estimated with PIMMs was around 36 percent. The absorption column density found in this source with our broadband analysis is fully consistent with the value found by Sazonov et al. (2005) in their analysis. Our broadband analysis shows evidence that this source is peculiar in many ways, as already described in Sect. 4.1. We measured the value of the high energy cutoff which is 40^{+160}_{-10} keV, the lowest value of our small sample. This very low value is probably due to the high upper limit to the reflection component <7; this high value suggests some different geometry than that used here to model the continuum reprocessed component.

IGR J12026-5349 The fraction of pile-up estimated with PIMMs was around 30 percent. Our analysis provides the absorption column density completely consistent with that published by Sazonov et al. (2005). The enhancement observed in the soft X-ray (either modelled with a thermal component or a scattered component) could suggest the presence of a starburst component. Our broadband analysis well constrains the high energy cutoff $E_c = 170^{+130}_{-50}$ keV, and we measured also a relative reflection $R = 1.3^{+5.7}_{-0.4}$.

NGC 788 The photon index measured with the model C is flatter with respect to the average value observed in Seyfert galaxies. This could be either intrinsic or due to the presence of a high energy cutoff below 100 keV. In fact, when fitting the data with model A, we found a photon index $\Gamma = 1.6$, fully consistent with that expected in type 2 AGN. Another possibility could be that the absorber is more complex than that proposed here, e.g. a partial covering. We were able to constraint the Compton reflection fraction $R = 0.9^{+1.3}_{-0.7}$.

ESO 103-G35 *INTEGRAL* data of ESO 103-G35 have been analysed by Molina et al. (2007), jointly with *Beppo-SAX* data from an observation performed in October 1996. Their data, however, referred to the 2th *INTEGRAL* catalogue (Bird et al. 2006), and had only a net exposure of 41 ks. Our results, which are obtained with a longer exposure, are in very good agreement with previous results. In particular the value they found for the high energy cutoff (68^{+71}_{-25} keV), perfectly matches our value (see Tables 3 and 4). They found an upper limit to the reflection fraction $R < 1.9$, again consistent with our result (see Table 4). *XMM-Newton* data of ESO 103-G35 have been analysed by Shinozaki et al. (2006) in 0.5–10 keV energy range. With their limited energy band it was not possible to obtain information about cutoff and reflection component, however the value of the intrinsic column density and the continuum shape they found is in very good agreement with the results of our broadband analysis. We stress that the possibility to cover the energy range above 10 keV allowed us to model all the spectral components and then to extract the intrinsic continuum shape.

IC 4518A In this object, the presence of the reflection component above 10 keV is statistically required by the data. However, the best fit value larger than 1 suggests that the geometry of the reflector has to be more complex than that used in this work. The large contribution of the reflection component above 10 keV is also confirmed by the fact that the fit with model B, without reflection component, gives a very flat photon index.

IGR J10404-4625 The presence of the reflection component above 10 keV is statistically required by the data, with $R = 1.1^{+2.4}_{-0.7}$. We were able to find a lower limit only to the high energy cutoff, $E_c > 120$ keV.

References

Akylas, A., Georgantopoulos, I., & Comastri, A. 2001, MNRAS, 324, 521
Anders, E., & Grevesse, N. 1989, GeCoA, 53, 197
Antonucci, R. R. 1993, ARA&A, 31, 473
Bassani, L., Dadina, M., Maiolino, R., et al. 1999, ApJS, 121, 473
Bassani, L., Molina, M., Malizia, A., et al. 2006a, ApJ, 636, L65
Bassani, L., Malizia, A., & Stephen, J. B. 2006b, for the INTEGRAL AGN survey team, 6th INTEGRAL Workshop The Obscured Universe, Moscow, 2–8 July 2006 [arXiv:astro-ph/0610455]
Beckmann, V., Gehrels, N., Shrader, C. R., & Soldi, S. 2006, ApJ, 638, 642
Bianchi, S., Guainazzi, M., & Chiaberge, M. 2006, A&A, 44, 499
Bird, A. J., Barlow, E. J., Bassani, L., et al. 2006, ApJ, 636, 765
Bird, A. J., Malizia, A., Bazzano, A., et al. 2007, ApJS, 170, 175
Corbet, E. A., Norris, R. P., Heisler, C. A., et al. 2002, ApJ, 564, 650
Davis, J. E. 2001, ApJ, 562, 575
Di Cocco, G., Caroli, E., Malizia, A., et al. 2003, A&A, 411, 189
Elitzur, M., & Shlosman, I. 2006, ApJ, 648, L101
Ghisellini, G., Haardt, F., & Matt, G. 2004, MNRAS, 267, 743
Gilli, R., Comastri, A., & Hasinger, G. 2007, A&A, 463, 79
Guainazzi, M., & Bianchi, S. 2007, MNRAS, 374, 1290
Guainazzi, M., Matt, G., & Antonelli, L. A. 1999, MNRAS, 310, 10
Haardt, F., & Maraschi, L. 1991, ApJ, 380, L51
Haardt, F., Maraschi, L., & Ghisellini, G. 1997, ApJ, 476, 620
Kirsch, M. G., Briel, U. G., Burrows, D., et al. 2005, SPIE, 5898, 22
Lebrun, F., Leray, J. P., Lavocat, P., et al. 2003, A&A, 411, 141
Malizia, A., Landi, R., Bassani, L., et al. 2007, ApJ, 668, 81
Masetti, N., Mason, E., Bassani, L., et al. 2006a, A&A, 448, 547
Masetti, N., Pretorius, M. L., Palazzi, E., et al. 2006b, A&A, 449, 1139
Masetti, N., Morelli, L., Palazzi, E., et al. 2006c, A&A, 459, 21
Massaro, E., Bianchi, S., Matt, G., D'Onofrio, E., & Nicastro, F. 2006, A&A, 455, 153
Matt, G., Guainazzi, M., Frontera, F., et al. 1997, A&A, 325, L13
Magdziarz, & Zdziarski 1995, MNRAS, 273, 837
Perola, G. C., Matt, G., Cappi, M., et al. 2002, A&A, 389, 802
Risaliti, G. 2002, A&A, 386, 379
Shinozaki, K., Miyaji, T., Ishisaki, Y., Ueda, Y., & Ogasaka, Y. 2006, ApJ, 131, 2843
Schurch, N. J., Roberts, T. P., & Warwick, R. S. 2002, MNRAS, 335, 241
Sazonov, S., Churazov, E., Revnivtsev, M., Vikhlinin, A., & Sunyaev, R. 2005, A&A, 444, L37
Ubertini, P., Lebrun, F., Di Cocco, G., et al. 2003, A&A, 411, 131
Vaceli, M. S., Viegas, S. M., Gruenwald, R., & de Souza, R. E. 1997, AJ, 114, 1345
Winkler, C., Courvoisier, T., Di Cocco, G., et al. 2003, A&A, 411, 1